Dynamics of Femtosecond Laser Interactions with Dielectrics

S.S. Mao, Fabien Quéré, Stéphane Guizard, X. L. Mao, R. E. Russo, Guillaume Petite, Philippe Martin

▶ **To cite this version:**

S.S. Mao, Fabien Quéré, Stéphane Guizard, X. L. Mao, R. E. Russo, et al.. Dynamics of Femtosecond Laser Interactions with Dielectrics. Applied physics. A, Materials science & processing, 2004, 79 (7), pp.1695. hal-00004161

HAL Id: hal-00004161
https://hal.science/hal-00004161

Submitted on 4 Feb 2005

HAL is a multi-disciplinary open access archive for the deposit and dissemination of scientific research documents, whether they are published or not. The documents may come from teaching and research institutions in France or abroad, or from public or private research centers.

L'archive ouverte pluridisciplinaire **HAL**, est destinée au dépôt et à la diffusion de documents scientifiques de niveau recherche, publiés ou non, émanant des établissements d'enseignement et de recherche français ou étrangers, des laboratoires publics ou privés.

Dynamics of Femtosecond Laser Interactions with Dielectrics

S. S. Mao[1,*], F. Quéré[2], S. Guizard[3], X. L. Mao[1], R. E. Russo[1], G. Petite[3], Ph. Martin[2]

[1] Lawrence Berkeley National Laboratory, University of California, Berkeley, CA 94720, U.S.A.

[2] Service des Photons, Atomes et Molécules, CEA/DSM/DRECAM, CEA Saclay, 91191 Gif-sur-Yvette Cedex, France

[3] Laboratoire des Solides Irradiés, CEA/DSM/DRECAM, Ecole Polytechnique, 91128 Palaiseau Cedex, France

** E-mail: ssmao@lbl.gov*

Abstract

Femtosecond laser pulses appear as an emerging and promising tool for processing wide band-gap dielectric materials for a variety of applications. This article aims to provide an overview of recent progress in understanding the fundamental physics of femtosecond laser interactions with dielectrics that may have the potential for innovative materials applications. The focus of the overview is the dynamics of femtosecond laser-excited carriers and the propagation of femtosecond laser pulses inside dielectric materials.

1. Introduction

Lasers that can produce coherent photon pulses with duration in the femtosecond regime have opened up new frontiers in materials research with extremely short temporal resolution and high photon intensity. The ultrafast feature of femtosecond lasers has been used to observe, in real time, phenomena including chemical reactions in gases [1] or electron-lattice energy transfer in solids [2]. In the meantime, the enormous intensity that femtosecond laser pulses achieve at its focus can create an energetic plasma that emits x-ray photons, which may have potential applications for characterizing microscopic transient structures of materials [3,4]

The conventional view of pulsed laser-material interactions, with wavelength between near infrared (IR) and near ultraviolet (UV), includes the transfer of electromagnetic energy to electronic excitation, followed by electron-lattice interactions that convert energy into heat. However, the processes of material response following intense femtosecond laser irradiation are far more complex, particularly for wide band-gap dielectrics. When a dielectric material is subject to intense femtosecond laser irradiation, the refractive index of the material may become intensity dependent, and a large amount of excited electrons may be generated by infrared pulses in "transparent" dielectrics. Relaxation channels of electronic excitation in wide band-gap materials may produce intrinsic defects, leading to photo-induced damages in the otherwise "defect-free" medium. These fundamentally nonlinear processes have stimulated substantial research efforts in both the understanding of the complexity of femtosecond laser interactions with dielectrics, and the applications of the underlying microscopic mechanisms to innovative materials fabrication. This article aims to provide an overview of recent progresses in understanding the fundamental physics of femtosecond laser interactions with dielectrics that are important for materials processing applications. Related topics of laser interactions with semiconductors (narrow-band materials) have been discussed in several excellent reviews [5,6].

As a source of energy in a highly concentrated form, lasers in general have become viable tools for material modification since their invention more than four decades ago. The increasing availability of intense femtosecond lasers is fueling a growing interest in high-precision materials processing. In contrast to material modification using nanosecond or longer laser pulses where standard modes of thermal processes dominate, there is almost no heat exchange between the pulse and the material during femtosecond laser-material interactions. Consequently, femtosecond laser pulses can induce non-thermal structural changes, driven directly by electronic excitation and associated nonlinear processes, before the material lattice has equilibrated with the excited carriers. This fast mode of material modification can result in vanishing thermal stress and minimal collateral damage for processing practically any solid-state material. Additionally, damages produced by femtosecond laser pulses are far more regular from shot to shot. These breakdown characteristics make femtosecond lasers ideal tools for precision material processing.

For femtosecond laser interactions with dielectrics, in addition to their classical value in elucidating the origin of laser-induced breakdown in optical materials, structural modifications of dielectrics are of particular significance to bulk micro-structuring that creates sub-wavelength "voxels". As an example, femtosecond laser pulses can be focused inside transparent dielectric materials in a layer-by-layer fashion. High-density, three-dimensional optical storage was achieved as the result of femtosecond laser-induced sub-micron structural transition that locally alters the refractive index at the laser pulse's focus [7-10]. Similarly, three-dimensional photonic band-gap lattices were realized by spatially organized micro-patterning of transparent dielectrics using femtosecond laser pulses [11].

Despite the promise of femtosecond laser pulses in processing wide band-gap dielectric materials for a variety of applications, understanding the fundamental aspects of intense femtosecond laser interactions with dielectrics has been a challenging task. It is the objective of this article to provide an overview of recent efforts towards uncovering the subtleties of femtosecond laser interactions with wide band-gap dielectrics, in

particular, the ultrafast time-resolved studies of the dynamics of electronic excitation and pulse propagation that are related to material modification.

The remaining of this article is organized as follows. The rest of section 1 offers a short review of individual basic physical processes involved in intense laser interactions with wide band-gap dielectrics. Detailed accounts of some time-resolved experiments on the dynamics of femtosecond laser-induced electronic excitation and relaxation (section 2), and the nonlinear optical processes associated with femtosecond pulse propagation (section 3) are presented in the next two sections. Section 4 is the summary.

1.1 Carrier excitation

The problem of carrier excitation and ionization in the case of wide band-gap materials subject to a laser electromagnetic field has been extensively addressed in the literature. The balance between different ionization channels during femtosecond laser interactions with dielectric materials is still under discussion. In the simplest case, the laser can deposit energy into a material by creating electron-hole plasma through single-photon absorption. However, for wide band-gap dielectrics, the cross-section of such linear absorption is extremely small. Instead, under intense femtosecond laser irradiation, nonlinear processes such as multiphoton, tunnel ionization, or avalanche ionization become the dominant mechanisms to create free carriers inside the materials.

- ***Photoionization***

For irradiation of wide band-gap materials using femtosecond laser pulses with wavelength near the visible (from near IR to near UV), a single laser photon does not have sufficient energy to excite an electron from the valence band to the conduction band. Simultaneous absorption of multiple photons must be involved to excite a valence band electron, with the resulting photoionization rate strongly depending on the laser intensity (**Figure 1a**). The rate of multiphoton absorption can be expressed as σI^m, where I is the laser intensity, σ is the cross section of m-photon absorption for a valence band

electron to be excited to the conduction band. The number of photons required is determined by the smallest m that satisfies the relation, $m\hbar\omega > E_g$, where E_g, is the band-gap energy of the dielectric material, $\hbar\omega$ is the photon energy. We emphasize here one feature of femtosecond laser irradiation: since femtosecond laser pulses offer higher peak intensities than conventional pulses, they reinforce intrinsic high order interband transitions in contrast to the ever-present defect-related processes (of a lower order).

A second photoionization process, tunneling ionization, may come into play during femtosecond laser interactions with dielectrics under an extremely strong laser field, for example, when the laser pulse is very short (e.g. < 10 fs). In this regime, the electric field of the intense laser pulse can suppress the Coulomb potential well that binds the valence electrons (band-bending). This allows the valence electrons to directly tunnel to the conduction band in a time shorter than the laser period. Both the multiphoton and the tunneling ionization can be treated under the same theoretical framework developed by Keldysh [12]. The transition from multiphoton to tunneling ionization is characterized by the Keldysh parameter [12], $\gamma = \omega(2m^*E_g)^{1/2}/eE$, where m^* and e are the effective mass and charge of the electron, and E is the intensity of laser electric field oscillating at frequency ω. When γ is much larger than one, that is the case for most materials-related investigations of laser interactions with dielectrics, multiphoton ionization dominates the excitation process.

- ***Free carrier absorption***

An electron being excited to the conduction band of a wide band-gap dielectric material can absorb several laser photons sequentially, moving itself to higher energy states where free carrier absorption is efficient (**Figure 1b**). The absorption coefficient α, which equals the inverse of the absorption depth, depends on the imaginary part of the refractive index κ; $\alpha = 2\omega\kappa/c$, where c is the light speed. The complex refraction index, $\tilde{n} = n + i\kappa$, is related to dielectric function $\tilde{\varepsilon}$, which, according to Drude model [13,14], can be expressed by,

$$\tilde{\varepsilon} = 1 - \omega_p^2 \left[\frac{\tau^2}{1+\omega^2\tau^2} + i \frac{\tau^2}{\omega\tau(1+\omega^2\tau^2)} \right],$$

with τ the scattering time typically a fraction of a femtosecond. For wide band-gap dielectrics under intense laser irradiation, strong electron interactions with the lattice are characterized by both the polar and nonpolar phonon scattering [15,16]. In the expression of $\tilde{\varepsilon}$, ω_p is the plasma frequency defined by,

$$\omega_p = \sqrt{\frac{e^2 N}{\varepsilon_0 m^*}},$$

where N is the carrier density, and ε_0 is the electric permittivity. In the cases where $\omega_p << \omega$, i.e., the carrier density is well below 10^{21} cm^3, the absorption coefficient can be derived as,

$$\alpha = \frac{\tau}{nc} \frac{\omega_p^2}{1+\omega^2\tau^2}.$$

When the electron density generated by photoionization reaches a high density (e.g., $\omega_p \sim \omega$), a large fraction of the remaining femtosecond laser pulse can be absorbed.

It is interesting to note that high energy (e.g., three times the band-gap energy) carriers can also be created in materials where electron-phonon scattering rate is low, such that multiple electron-phonon collisions could not occur in one laser pulse. Carrier heating could be produced through direct interbranch single or multiphoton absorption, in a way quite similar to the valence-to-conduction interband absorption discussed above. In all materials, both processes should certainly be taken into account, which one dominates depending essentially on the strength of the electron-phonon coupling.

- ***Avalanche ionization***

Avalanche ionization involves free carrier absorption followed by impact ionization (**Figure 1c**). As the energy of an electron in the high energy states exceeds the conduction band minimum by more than the band-gap energy, it can ionize another electron from the valence band, resulting in two excited electrons at the conduction band

minimum [17, 18]. These electrons can again be heated by the laser field through free carrier absorption, and, once they have enough energy, impact more valence band electrons. This process can repeat itself as long as the laser electromagnetic field is present and intense enough, leading to a so-called electronic avalanche. The growth of the conduction band population by this avalanche process has the form βN, where β is the avalanche ionization rate, a phenomenological parameter that accounts for the fact that only high energy carriers can produce impact ionization.

Avalanche ionization requires seed electrons to be present in the conduction band, which can for instance be excited by photoionization. The following rate equation has been proposed to describe the injection of electrons in the conduction band of dielectrics by femtosecond to picosecond laser pulses, under the combined action of multiphoton excitation and avalanche ionization [19],

$$\frac{dN}{dt} = \alpha IN + \sigma NI^m,$$

where α is a constant. For dielectric materials in which free carrier losses (e.g. self-trapping and recombination) occur on a time scale comparable to femtosecond laser pulse duration (e.g., quartz and fused silica), this population equation should be modified as follows,

$$\frac{dN}{dt} = \alpha IN + \sigma NI^m + \sigma_x pI^{m_x} - \frac{N}{\tau_x},$$

$$\frac{dp}{dt} = -\sigma_x pI^{m_x} + \frac{N}{\tau_x}.$$

In the above expressions, contribution from self-trapped excitons (see section 1.3) of density p that builds up during the pulse duration is included (which may in some cases be bimolecular recombination, depending on the carrier density) [20,21]. σ_x is the multiphoton cross section (of order m_x) for self-trapped excitons and τ_x is the characteristic trapping time. A schematic illustration of the effect of the self-trapping on femtosecond laser excited electron population is shown in **Figure 2**.

More recently, variations of the classical avalanche process that may play a role for sufficiently short laser pulses (e.g., < 40 fs) have been investigated theoretically [22]. One such mechanism is collision-assisted multiphoton avalanche, in which some valence electrons are excited to the conduction band by conduction electrons with energy smaller than the threshold for impact ionization, by absorbing several laser photons during inelastic electron-electron collisions. Another mechanism is hole-assisted multiphoton absorption, which is similar to the so-called enhanced ionization of molecules in strong laser fields [23]. Through its Coulomb field, a hole exponentially enhances the multiphoton absorption rate of atoms at adjacent lattice sites. As soon as new holes are created, they continue the same trend that could lead to a collision-free electronic avalanche.

1.2 Nonlinear propagation

When a laser pulse propagates through a dielectric material, it induces microscopic displacement of the bound charges, forming oscillating electric dipoles that add up to the macroscopic polarization. For isotropic dielectric materials such as fused silica, the resulting index of refraction (real part) can be derived as [24],

$$n = \sqrt{1 + \chi^{(1)} + \frac{3}{4}\chi^{(3)}E^2} \ .$$

where $\tilde{\chi}^{(1)}$ and $\tilde{\chi}^{(3)}$ are the linear and nonlinear susceptibility, respectively. In a more convenient form,

$$n = n_0 + n_2 I \ ,$$

where $I = \frac{1}{2}\varepsilon_0 c n_0 E^2$ is the laser intensity, $n_0 = \sqrt{1+\chi^{(1)}}$ and $n_2 = 3\chi^{(3)}/4\varepsilon_0 c n_0^2$ are the linear and nonlinear part of the refractive index, respectively. A non-zero nonlinear refractive index n_2 gives rise to many nonlinear optical effects as an intense femtosecond laser pulse propagates through dielectric materials.

- ***Self-focusing and Self-phase modulation***

The spatial variation of the laser intensity $I(r)$ can create a spatially varying refractive index in dielectrics. Owing to typical Gaussian spatial profile of a femtosecond laser pulse, the index of refraction is larger towards the center of the pulse. The spatial variation of n causes lens-like effect that tends to focus the laser beam inside the dielectrics (**Figure 3a**). If the peak power of the femtosecond laser pulse exceeds a critical power for self-focusing [24,25], $P_{cr} = 3.77\lambda^2 / 8\pi n_0 n_2$, the collapse of the pulse to a singularity is predicted. Nevertheless, other mechanisms such as defocusing due to nonlinear ionization will always balance self-focusing and prevent pulse collapse inside dielectric materials.

As the result of spatial self-focusing, the on-axis intensity of femtosecond laser pulses inside dielectrics, especially at its temporal peak, can be significantly larger than its original value. Consequently, the pulse may be sharpened (pulse sharpening) temporally with a steeper rise and decay of the temporal profile [26].

Since the intensity $I(t)$ of femtosecond laser pulses is highly time-dependent, the refractive index depends on time. Analogous to self-focusing, the phase of the propagating pulse can be modulated by the time-domain envelope of the pulse itself (self-phase modulation). With a non-zero nonlinear refractive index n_2, the derivative of the phase $\Phi(z,t)$ of the pulse with respect to time becomes [24],

$$\frac{d\Phi}{dt} = \omega - \frac{n_2 z}{c}\frac{dI(t)}{dt}.$$

The time-varying term of the phase produces frequency shifts that broaden the pulse spectrum as illustrated in **Figure 3b**. Spectral broadening depends on the nonlinear index of refraction n_2 and the time derivative of the laser pulse intensity, and for a time-symmetric pulse, the broadening will also be symmetric in frequency. Nevertheless, experimentally observed spectral broadening is seldom symmetric, due to processes such as photoionization, which also gives rise to a time-dependent refractive index.

- ***Plasma defocusing***

As various nonlinear ionization mechanisms generate an electron-hole plasma inside wide band-gap dielectric materials, this plasma has a defocusing effect for femtosecond laser pulse propagation. The electron density is the highest in the center of the pulse and decreases outward in the radial direction due to typical Gaussian spatial intensity profile. The real part of the refractive index is modified by the generation of the electron-hole plasma (for $\omega_p/\omega << n_0$) [24],

$$n = n_0 - \frac{N}{2n_0 N_c},$$

where $N_c = \omega^2 \varepsilon_0 m^*/e^2$, defined as the characteristic plasma density for which the plasma frequency equals to the laser frequency. It is clear that the presence of electron-hole plasmas results in a decrease in the refractive index, in contrast to the Kerr effect. As a result, the refractive index is the smallest on the beam axis and the beam is defocused by the plasma, which acts as a diverging lens, balancing self-focusing.

1.3 Defect Generation

In general, energy from intense femtosecond laser pulses absorbed by a solid material can be converted into elementary electronic excitations – electrons and holes, which relax and reduce their energy inside the solid through both delocalized and localized carrier-lattice interaction channels [27,28]. For some wide band-gap dielectric materials, the most important relaxation mechanism is the localization of the energy stored in the electron-hole pair that creates self-trapped carriers, especially self-trapped excitons (STE's), which provide energy necessary for localized lattice re-arrangement and thus, defect accumulation.

- ***Excitons***

Through nonlinear ionization, the interaction of an intense femtosecond laser pulse with wide band-gap dielectrics causes electronic excitations that promote an electron from the valence band to the conduction band, leaving a hole in the valence band. An electron and a hole may be bound together by Coulomb attraction, which is

collectively referred to as an exciton, a concept of electrically neutral electronic excitation [29]. **Figure 4** shows a schematic of exciton energy levels in relation to the conduction band edge. While excitons can be either weakly or tightly bound, in wide band-gap materials with typically small dielectric constant, they are strongly bound and localized near a single atom. Excitons may be promoted by inelastic scattering [30] of the excited electrons that slows the electrons in the conduction band **(Figure 4a)**, or by direct resonant absorption of multiple photons **Figure 4b**. The binding of electron-hole pairs into excitons is a very fast process, which is often smaller than 1 ps in wide band-gap materials [28].

Excitons are unstable with respect to their recombination process; they can relax through delocalized and localized channels. For wide band-gap dielectrics that are strong-coupling solids, localized trapping mechanism rather than scattering is more probable for excitons. Consequently, the electronic excitation energy in these materials is localized by the creation of STE, which is formed as the result of free exciton relaxation, or when a self-trapped hole traps an electron [31].

- ***Exciton self-trapping***

The major interest in STE in dielectrics comes from the fact that they are a means of converting electronic excitation into energetic atomic processes such as defect formation. Self-trapping generally describes carriers localized on a lattice site initially free of lattice defects (e.g., vacancies, interstitials, or impurities). A charged carrier in a deformable lattice creates an attractive potential well [31]; the trapping results from small atomic displacement that deepens the potential well in which the carrier resides. In general, localized lattice deformation may result from short-range covalent molecular bonding or long-range electrostatic polarization associated with ion displacements. Thermal fluctuations can provide the energy for at least one particular lattice site with enough instantaneous deformation for the self-trapping to begin.

Excitons can be trapped by their interactions with lattice distortion to form STE's. Holes may also be trapped at the distortion of lattice, which, after trapping an electron, create a STE. Materials that display self-trapping are predominantly insulators with wide band-gaps, such as alkali halide and SiO_2. In alkali halide crystals [32], which have an energy band-gap ranging from 5.9 eV (NaI) to 13.7 eV (LiF), a self-trapped exciton consists of an electron bound by the Coulomb field of the surrounding alkali ions and a hole that occupies an orbital of a halogen molecular ion (X_2^-). Similarly in SiO_2, which is constructed from SiO_4 tetrahedrals with silicon at the center and an oxygen atom at each of the four corners [33], the self-trapping process is accompanied by a strong distortion of the SiO_2 lattice. Weakening of the Si-O-Si bond yields an oxygen atom leaving its equilibrium position in the tetrahedral, forming silicon and oxygen dangling bonds. The hole of the self-trapped exciton stays on the oxygen dangling bond and the electron is on the silicon dangling bond.

Energy transport of STE's is by means of hopping diffusion rather than by band-like mode. As STE's recombine, they produce a characteristic luminescence that can be studied by time-resolved spectroscopy [34-36]. For example, high purity quartz emits a blue luminescence (~ 2.8 eV) under irradiation, which corresponds to a large Stokes shifts relative to the band gap [37]. For wide band-gap dielectric materials, the localized relaxation channel that leads to the production of STE's is correlated with the formation and accumulation of transient and permanent lattice defects.

- ***Origins of intrinsic defects***

Optical excitation can be sufficient to generate vacancies and interstitials in perfect dielectric lattices. Defect formation may be classified as extrinsic or intrinsic type depending on whether the defect is derived from a precursor. Recent advances [27] in the study of STE's structures have provided the basis for a new level of understanding of the mechanisms of intrinsic defect formation. In the absence of exciton self-trapping, electronic excitation would remain completely delocalized in a perfect dielectric material. Exciton self-trapping can provide the energy required (in eV) to initiate intrinsic defects,

including vacancy-interstitial pairs where an atom is displaced in the course of the decay of electronic excitations.

Excitonic mechanisms of defect formation are well established in laser-irradiated halides and SiO_2, among many other wide band-gap materials with strong electron-lattice couplings. F-centers and H-centers [27] are the primary defects that are the immediate products of self-trapped exciton decay in alkali halides **(Figure 5)**. After initial nonlinear ionization that generates electron and holes, the process of defect formation starts from exciton creation, followed by self-trapping of the exciton. An isomeric transformation occurs from a self-trapped exciton to a Frenkel defect pair comprising an F-center, a halogen vacancy with a bound electron, and an H-center, an interstitial halogen ion bound to a lattice halogen ion by a hole. Off-center relaxation is the crucial step toward decomposition of the self-trapped exciton, as a self-trapped exciton is gradually changed to a stable vacancy-interstitial defect pair by displacing the H-center away from its point of creation, out of the range for recombination with the electron wave function bound to the F-center.

In SiO_2, the E' (oxygen vacancy) and non-bridging oxygen-hole centers (NBOHC) [27] are the analog of the F-H centers in alkali halides **(Figure 6)**. The oxygen vacancy in SiO_2 is essentially a dangling silicon bond [Si·]. The displaced oxygen atom goes into the non-bridging oxygen-hole center state [Si-O·] which may end up in a peroxy linkage [Si-O-O-Si] or radical [Si-O-O·], an isomer of a self-trapped exciton after covalently coupling to another oxygen atom at an interstitial site. **Figure 6** also shows a simplified energy level diagram of SiO_2 (silica) upon laser irradiation. The point defects resulted from decay of self-trapped excitons add more energy levels, in analog to the effect of impurities.

As the result of intense femtosecond laser irradiation, when the electronic defects resulted from the decay of self-trapped excitons grow in number, defect clusters may form, which can yield macroscopic structural damage in the material. In addition,

significant transient volume increase associated with exciton self-trapping could create a shock wave-like perturbation that eventually damages the otherwise perfect lattice.

- ***Damage of dielectrics***

Laser-induced damage in wide band-gap dielectric materials is known to be an extremely nonlinear process. There is no doubt that damage in pure wide band-gap materials is associated with rapid buildup of conduction electrons. A large number of experimental and theoretical studies have been performed to determine the damage mechanisms, with a majority of these efforts focused on the damage or breakdown threshold as a function of the laser pulse duration. It is well established that for pulse durations of 10 picoseconds or longer when thermal diffusion comes to play, the threshold laser fluence (energy density) for material damage depends on laser pulse duration [19,38,39] following a $\sqrt{\tau_{laser}}$ scaling. Nevertheless, for femtosecond laser interactions with wide band-gap dielectrics, when the pulse duration is much shorter than the characteristic time for thermal diffusion, the damage threshold deviates from such square root scaling (**Figure 7**).

There have been many theoretical attempts [19,39,40] aimed at determining the mechanism of femtosecond laser-induced dielectric breakdown. However, the relative role of different ionization and relaxation channels in femtosecond laser-induced dielectrics breakdown, in particularly near the damage threshold, is far from fully understood. Several mechanisms can be foreseen that may lead to damage or optical breakdown of a defect-free dielectric material under femtosecond laser excitation. Damage could be caused by melting or vaporization of the solid, following the strong phonon emission by the laser-generated conduction electrons. Coulomb explosion was also proposed as a mechanism to explain single shot ablation by femtosecond laser pulses [41,42]. This hypothesis is supported by the measurement of the velocity of doubly charged ions O^{2+}, which is twice the velocity of singly charged ions (O^{+}) in the damage of Al_2O_3 [41]. Damage can also be due to the outcome of generation and accumulation of intrinsic defects such as vacancy-interstitial pairs. As discussed before,

creation and decay of STE's in dielectrics are at the origin of the intrinsic defects. It is well known that single shot and multiple shot ablation threshold differ by a factor of approximately two. This suggests that the first laser shots induce a large concentration of defects in the material lattice that modifies the interactions of the subsequent pulses. In this case, the energy distribution of ions at the surface does not correspond to coulomb explosion [41], but rather to a Maxwell-Boltzmann distribution, indicating a thermalization process within the dense plasma before desorption. Theoretical models that describe femtosecond laser-induced optical breakdown in perfect dielectrics should implement the evolution of excitons (formation, self-trapping, and relaxation), as well as different ionization and delocalized recombination mechanisms. No such comprehensive model exists to the best of our knowledge [43].

In the next two sections, we will provide more detailed accounts of some recent progresses on two related subjects, femtosecond laser induced carrier dynamics and femtosecond laser pulse propagation in dielectrics.

2. *Femtosecond laser induced carrier dynamics*

- ***Imaging experiments***

One simple method to study femtosecond laser-induced carrier excitation in (transparent) dielectrics is ultrafast imaging. Experiments [44] were performed using a femtosecond time-resolved pump-probe setup to image the electron-hole plasma. A high power femtosecond laser at its fundamental wavelength (800 nm) was used as the pump beam, which has a duration of approximately 100 femtosecond (FWHM). The 800 nm laser beam was focused to a spot size of 50 μm in diameter onto a silica glass sample using an f = 15 cm focal-length lens. After a beam splitter, one arm of the 800 nm output passes an optical delay stage and a KDP crystal, forming a probe beam at 400 nm that is perpendicular to the excitation laser pulse. By moving the delay stage, the optical path of the probe beam can be varied, so the time difference between the pump beam and the

probe beam is changed. Time zero was set when the peaks of the ablation laser beam and the probe beam overlapped in time at the sample surface. The resulting shadowgraph images represent spatial transmittance of the probe pulse during laser irradiation of the sample, corrected for background intensity measured without laser excitation. Electron number density of the laser-induced plasma inside the silica can be estimated from the transmittance at various delay times.

Figure 8a shows a series of time-resolved images of the electron-hole plasma at the same laser irradiation I = 1.3 x 10^{13} W/cm^2. At t = 0, only a small dark area appears close to the glass surface that results from electron excitation by the leading edge of the femtosecond laser pulse. At longer delay times, plasma filament grows longer, with the darkest section (strongest absorption) moving away from the glass surface into the bulk. From measuring the probe pulse transmittance I_{p0}/I_{pd} of the time-resolved images, one can estimate the femtosecond laser-excited plasma electron number density inside the silica glass at different delay times.

The electron number density of the laser-induced plasma shown in **figure 8a**, was plotted in **figure 8b**. At t = 333 fs, there is an electron number density maximum (~ 2 x 10^{19} cm^{-3}) at z = 80 μm, which moves into the silica at later times. While the peak value of the electron number density increases with time, it reaches a maximum of approximately 5 x 10^{19} cm^{-3} at t = 1333 fs. This observation is consistent with the fact that a femtosecond laser pulse experiences initial self-focusing inside a dielectric material, followed by defocusing when the laser-induced electron excitation is strong enough to compensate the laser-induced refractive index change.

The density of the laser-induced electron-hole plasma as obtained from ultrafast imaging provides only an order-of-magnitude estimate or semi-quantitative information. Frequency domain interferometry proves to be a powerful technique to elucidate the fundamental processes of femtosecond laser-induced carrier dynamics in dielectric materials.

- ***Interferometry experiments***

While imaging experiments give access to the change of the imaginary part of the refractive index induced by a pump laser pulse, the change in the real part of the refractive index also provides essential information on the dynamics of excited carriers in dielectrics. Interferometry is the natural tool to access this quantity. A very powerful interferometric technique when dealing with broadband light sources is spectral interferometry, which has been increasingly implemented with ultra-short laser pulses for a wide variety of experiments, e.g. for the full temporal characterization of these pulses (SPIDER technique) [45,46] or for time-resolved experiments, especially in laser-generated plasmas [47]. Note that a technique combining the features of interferometric measurements (in real space) and that of shadowgraphy [48] has also been implemented in the case of picosecond pulses, and could be in principle, with minor modifications, applied to femtosecond pulses.

The spectral or frequency domain interferometry technique uses two pulses, separated in time by a delay τ large compared to their duration and sent in a spectrometer. Provided the spectral resolution of the spectrometer is much larger than the inverse of the delay, the measured spectrum is therefore,

$S(\omega) = 2S_0(\omega)[1 + \cos(\omega\tau + \Phi)]$.

For the sake of simplicity, the two delayed pulses were assumed to be identical ("twin pulses") to derive this expression, a condition which is actually not required for this technique to apply. $S_0(\omega)$ is the spectral intensity of these pulses, and Φ their relative phase. Since τ is large compared to the spectral width of $S_0(\omega)$, $S(\omega)$ presents fringes, spaced by $2\pi/\tau$. The position of these fringes is determined by the relative phase Φ of the two pulses.

Spectral interferometry can be used to probe the temporal dynamics of a system perturbed by a pump pulse. In this case, the first pulse probes the system before the pump pulse, and is thus used as a reference pulse. The second pulse probes the system at a delay t after the pump pulse. The perturbation induced by the pump pulse leads to a

change ΔΦ(t) of the relative phase of the twin pulses. This phase shift ΔΦ results in a shift of the fringes in the spectrum of the twin pulse. Spectral interferometry uses this shift to measure ΔΦ. This technique has been used to probe laser-excited dielectrics (**Figure 9**) [49]. The twin pulses are transmitted through the dielectric sample. One interferogram is acquired without any pump pulse, as the reference. A second one is measured with an intense pump pulse exciting the dielectric between the reference and the probe pulse. In this configuration, the phase shift ΔΦ(t) is given by

$$\Delta\Phi(t) = (2\pi L / \lambda)\Delta n(t)$$

where λ is the probe beam wavelength, L the length of the probed medium (assumed to be homogeneously excited for simplicity), and $\Delta n(t)$ the instantaneous change in the real part of refractive index, that results from the pump-induced excitation. Note that, by using the contrast of the fringes, spectral interferometry also gives access to the change in absorption coefficient, *i.e.* to the change in imaginary part of the refractive index.

Two types of temporal behavior of ΔΦ(t) have been observed (**Figure 10**). In all cases, ΔΦ(t) is positive for short delays, when the pump and the probe temporally overlap in the dielectric, because of the pump-induced optical Kerr effect. ΔΦ(t) then becomes rapidly negative; according the Drude model, it is due to the injection of electrons in the conduction band (see section 1, plasma defocusing). In some solids (*e.g.* MgO in **Figure 10**), ΔΦ(t) remains negative for several tens of ps, while in some others (*e.g*. SiO_2 in **Figure 10**), it becomes positive again. In SiO_2, this relaxation occurs with a time constant of 150 fs. It has been demonstrated that this second type of evolution is due to the trapping of most of the excited carriers as self-trapped excitons [49]. Since STE's correspond to localized states, the change in refractive index is given by the Lorentz model,

$$\Delta n = \frac{N_{STE} e^2}{2 n_0 m \varepsilon_0} \frac{1}{\omega_{tr}^2 - \omega^2}$$

where N_{STE} is the STE density, n_0 the refractive index of the unperturbed solid, ω_{tr} the resonance frequency of the STE's first excited level (~ 4.2 eV in SiO_2), and ω the probe

laser central wavelength. If $\omega < \omega_{tr}$, as is the case for the SiO_2 data in **Figure 10**, the presence of STE's leads to a positive phase shift.

These measurements have provided important information on the ultrafast dynamics of excited carriers in dielectrics [49]. In diamond, MgO and Al_2O_3, the negative phase shift was observed to persist for tens of ps. This suggests that no trapping occur on this timescale, or that the electrons form very shallow traps. Fast formation of STE's has been observed in NaCl, KBr, and SiO_2 (both amorphous and crystalline), leading to carriers lifetimes two orders of magnitude smaller. The difference in carrier dynamics can be qualitatively explained by general considerations about the STE's formation, in terms of lattice elasticity and deformation potential. A fundamental difference was also observed between the trapping kinetics in NaCl and SiO_2: while the trapping time was independent of the excitation density in SiO_2, carriers in NaCl trap faster when the excitation density is higher. This can be interpreted as an evidence of direct exciton trapping in SiO_2, and of hole trapping followed by electron trapping in NaCl [49].

For intense ultrashort laser interactions with dielectrics [50], the phase shift $\Delta\Phi_\infty$ measured at a sufficiently large delay after the laser pulse (see arrows on **Figure 10**) gives access to the excitation density N in the solid at the end of the laser pulse. If this density is not too high, $\Delta\Phi_\infty$ is directly proportional to N. **Figure 11** presents the evolution of $\Delta\Phi_\infty$ with the incident peak intensity I of a 790 nm ($\hbar\omega = 1.57$ eV), 60 fs pump pulse, in two dielectric solids. On the right-hand scale, the corresponding excitation density N is given, assuming a homogeneously excited medium. At low intensity, $\Delta\Phi_\infty$ is observed to vary as I^6 in SiO_2 and as I^5 in MgO. The exponents of these power laws correspond in both cases to the minimum number of photons that the valence electrons have to absorb to be injected in the conduction band ($6\,\hbar\omega = 9.42$ eV $> E_g(SiO_2) \approx 9$ eV, $5\,\hbar\omega = 7.85$ eV $> E_g(MgO) \approx 7.7$ eV). This proves that the dominant excitation process in this intensity range is perturbative multiphoton absorption by valence electrons. The optical breakdown threshold of SiO_2 measured at 800 nm and 60 fs in [19] falls within this range, suggesting that optical breakdown is not associated with an electronic avalanche. However, this result is in contradiction with the conclusions drawn from

breakdown threshold measurements [19], which suggest that the electronic avalanche should dominate multiphoton absorption even in the femtosecond regime. A model of optical breakdown conciliating these two studies remains to be found.

At higher intensities, a saturation of $\Delta\Phi_\infty$ is observed compared to these power laws. This saturation occurs because at high intensity, the pump beam is strongly absorbed due to free-carrier absorption by conduction electrons, and even reflected by the target when the electron density becomes higher than the critical density at the pump frequency. Thus, in this regime, it is only in a thin layer (~ 200 nm) of material that the excitation density keeps increasing with intensity. In this range, the occurrence of electronic avalanche, due to the strong heating of the conduction electrons, cannot be excluded, although the data can be fitted with a purely multiphoton injection law [50]. Since the density only increases with intensity in a very thin layer, the sensitivity of the technique to these variations might be too low to distinguish between different excitation processes.

- ***Time resolved absorption***

STE creation by self-trapping of an electron-hole pair can be monitored using transient absorption spectroscopy, which consists of measuring at different delay after electron-hole injection the sample absorption, and monitoring the appearance of selected absorption bands. In some materials such as SiO_2, for which the absorption lies in the UV, it is only possible to perform single wavelength measurements [36]. **Figure 12** shows the rise time of the SiO_2 STE absorption measured at the top of its 5.2 eV absorption band.

In alkali halides, where the absorption bands lie in the visible, it is possible to use as a probing pulse a White Light Continuum (WLC) generated by focusing an intense subpicosecond laser pulse in, e.g., a water cell. Due to various non-linear effects, the spectrum of the laser pulse is broadened and can essentially cover the whole visible range so that a full absorption spectrum can be recorded simultaneously for each laser shot.

Figure 13 shows such absorption spectra measured in KCl, at two temperatures [51]. At 6K, one observes the appearance of a single absorption band that can be shown to relate to the STE formation (just as in the case of SiO_2 above). At 80 K, at short delays, one also observes the appearance of the STE absorption, but after a few picoseconds, a second band appears. It is due to the transformation of some of the STE into a permanent F-center. This method has now been applied to a large number of alkali halides [52,53] and has considerably helped, together with the above-mentioned interferometric measurements, unraveling the difficult issue of the so-called "excitonic" mechanisms of point defect creation in irradiated wide band-gap dielectrics.

- ***Theoretical considerations***

While experimental detection of laser-induced ultrafast carrier dynamics advances rapidly, theoretical calculation of the dynamics in strong-coupling solids is still limited. One primary challenge is the appropriate approach to calculate nonequilibrium carrier distributions in dielectrics in response to intense femtosecond laser excitation.

The main difficulty comes from the very strong electron-phonon coupling in the conduction band of wide band-gap dielectrics, which is an essential feature of these materials. For the longitudinal optical (LO) phonons, this coupling is measured with the well-know quantity α defined as $\alpha = \frac{e^2}{\hbar}\left(\frac{m^*}{2\hbar\omega_{LO}}\right)^{1/2}\left(\frac{1}{\varepsilon_\infty}-\frac{1}{\varepsilon_0}\right)$. It depends [54] on the dielectric properties of the material $(\varepsilon_0, \varepsilon_\infty)$, the LO phonon energy at the center of the Brillouin zone (ω_{LO}), and the electron effective band mass (m^*), and it ranges from 6 x 10^{-2} for semiconductors as GaAs (perturbative regime) to values larger than unity for SiO_2, and even 5 for NaCl.

To calculate the temporal evolution of a given electron distribution function corresponding to an energy in excess with respect to the bottom of the conduction band,

one generally uses the so-called Boltzmann equation approach. This semi-classical approach implies the acceptance of two very strong hypotheses. First, one must first suppose that the evolution process is Markovian, i.e., the evolution of the system after *t* depends only on its state at this time and not before (the system has no memory). Second, it is necessary to calculate a mean time-independent collision rate $W(\boldsymbol{k},\boldsymbol{k'})$ with the Fermi golden rule, which gives the probability per unit of time for the system to reach a state $\boldsymbol{k'}$ starting from $\boldsymbol{k}$ and implies a strict energy conservation.

For the case of Quartz [55], to simplify the discussion, we neglect any exchange and correlation interaction among electrons, or Coulombic interaction with the holes, the trapping process or interactions with an impurity, and also, due to relatively low electronic density, any degeneracy connected to the exclusion principle. The evolution equation writes,

$$\frac{\delta f(k,t)}{\delta t} = \int dk \left\{ W(k',k) f(k',t) - W(k,k') f(k,t) \right\}.$$

This equation, also called the master equation, makes for each time the balance between the population and depopulation of the states $\boldsymbol{k}$ of the system [56].

We consider as an example, a seven photon injection process (1.57 eV photons) in a quartz sample with band-gap of 9.8 eV. Then, the initial kinetic energy of the electrons in the conduction is about 1.2 eV. We want to focus on the relaxation of these electrons through electron-phonon coupling, and we therefore neglect the influence of the laser field (and in particular free-carrier absorption), assuming that this field is quickly switched off. We consider only the two most active LO phonons branches (150 meV and 60 meV), assuming a flat dispersion curve. The coupling is calculated using the well known Frölich [57] Hamiltonian, and the transition rates are obtained, as discussed above, using the Fermi golden rule. The energy is lost by quanta corresponding to the two considered branches. The equilibrium is reached after 50 fs (**Figure 14**) and it corresponds to a Maxwell-Boltzmann distribution (defined as an exponential with a mean energy 3/2 $k_B T$).

At this stage, an important comment is necessary: the semi-classical approach has, by construction, no memory. A description based on this assumption is correct if an event (a collision with a phonon) is over before the next one starts. The collisions must then be successive and independent. This is not true in the case of conduction electrons in SiO_2; because of the strong electron-phonon coupling (large α), the mean collision time τ is smaller than 1 fs. We can also calculate the "duration" of a collision as the time required for the energy to be conserved. For the 150 meV branch, we find $1/\omega_{LO} \sim 5$ fs. According to theses two parameters, a collision starts before the end of the previous one. This strongly suggests that the semi-classical approach no longer applies.

The full quantum approach based on the evolution of the density matrix does not require energy conservation at each collision. In addition, a Markovian assumption is no longer necessary. This approach has been utilized in the case of semiconductors and is detailed in [58]. One generally starts from the single particle density matrix evolution equation,

$$\frac{\mathrm{d}}{\mathrm{dt}}\left\langle \mathrm{c}_{\mathrm{k}}^{+}\mathrm{c}_{\mathrm{k}} \right\rangle = \frac{1}{\mathrm{i}\hbar}\left\langle \left[\mathrm{c}_{\mathrm{k}}^{+}\mathrm{c}_{\mathrm{k}}, \mathrm{H}\right] \right\rangle .$$

H is the Frölich Hamiltonian and $\left\langle c_k^+ c_k \right\rangle = f(k)$ is the distribution function that we want to calculate. It is well known that the set of equation derived from the above evolution equation is infinite [59]. Strictly speaking, the problem cannot be computed. We must truncate the set of coupled differential equations somewhere. In the calculation detailed in [55], the average of a product of four operators (two for the electrons and two for the phonons) has been factorised in two products of two operators, each of them acting respectively on the electron and the phonons: $\left\langle c_{k+q-q'}^{+} c_k b_q^{+} b_{q'} \right\rangle = f(k) n_q \delta_{qq'}$. In this expression, b_q^+ and $b_{q'}$ are the operator for the creation (destruction) of a phonon q (q'). Because we consider that the average of a product is the product of the average, this is equivalent to neglecting the fluctuations in establishing equilibrium. The difference between this approach and the semi-classical one is illustrated in **Figure 14**. It clearly takes more time in the quantum approach for the carriers to relax. This can be understood

because, as the memory is conserved, it takes more time to reach an equilibrium state that is by definition universal and thus free of memory.

The above example underlines the tremendous challenge that one faces to properly calculate the evolution of an electronic distribution in a nonequilibrium state under the condition of strong coupling. Even in this oversimplified model where a simple parabolic dispersion relation for the electrons and a flat one for the LO phonons are applied, it is not an easy task to calculate ultrafast carrier dynamics from a practical as well as from a conceptual point of view. There is a need in developing a microscopic theory based on the quantum approach that quantitatively describes the ultrafast carrier dynamics resulted from femtosecond laser excitation in dielectrics.

Recent progresses of *ab initio* electronic structure calculations [60], which can nowadays quite exactly reproduce experimental properties such as photoabsorption, photoemission or electron energy loss spectra, all properties pertaining to the excited states, without the use of any adjustable parameter, offer some hope concerning electronic excitation in dielectrics. Many-body quantum calculations presently correctly calculate the real part of quasiparticle (in our case, laser-excited carrier) self energy, it is only a matter of time to obtain the corresponding imaginary part, which will provide a solution to the problem that accounts for all electron-electron and electron-hole relaxation processes. Electron lattice interactions are not currently included in such formalisms, but they could be accounted for once some recent methodological progress in the field of time-dependent density functional theory (TDDFT), a general framework for studying non-stationary electronic processes [61], are to be fully exploited.

3. Femtosecond laser pulse propagation

There has been a growing interest in femtosecond laser propagation in wide band-gap dielectrics as the laser intensity can be much higher than the threshold for self-focusing. At such high intensities, the dynamics of femtosecond pulse propagation is

considerably more complex, as it may be accompanied by nonlinear phenomena such as pulse splitting in both space and time domains. Spatial or temporal splitting of femtosecond laser pulses offers a mechanism for intense femtosecond laser propagation inside dielectrics without encountering catastrophic damage caused by self-focusing (see section 1.2).

- ***Self-focusing and defocusing***

Femtosecond laser induced nonlinear self-focusing as well as related filamentation process has been investigated for decades, for example, in air [62,63]. The nonlinear Schrödinger equation with the inclusion of multiphoton ionization can describe many aspects of the filamentation phenomenon [64]. However, there are relatively few femtosecond time-resolved studies of laser self-focusing and filamentation inside wide band-gap dielectrics. **Figure 8** provides the direct evidence of strong self-focusing of a femtosecond laser pulse inside a silica glass at different times. The width of the filaments decreases as the laser pulse propagates into the sample.

Although self-focusing occurs during femtosecond laser propagation, the density of free electrons at the focus does not increase indefinitely. Rather, the density reaches a saturation value after about 1500 fs propagation into the sample (~ 250 μm inside), as shown in **Figure 15**. This phenomenon happens to be the consequence of self-defocusing process caused by the generation of an electron-hole plasma, as discussed in section 1.2. The balance between self-focusing due to the nonlinear Kerr effect and defocusing due to plasma formation can lead to self-channeling of the femtosecond laser pulse inside dielectrics [65,66], if the beam radius is such that ionization comes into play before spatial splitting and material damage occur.

- ***Spatial splitting***

When self-focusing is strong, a single input pulse can break up into several narrow filaments of light. Because the Gaussian spatial profile of the pulse is destroyed

by self-focusing, the pulse cannot be focused to a diffraction-limited size. **Figure 16** shows a series of shadowgraph images inside a silica sample taken at the same delay time (2000 fs) but at different laser intensities I. At I = 5 x 10^{12} W/cm^2, there is only one filament, a thin, dark stripe which results from the absorption of the probe beam by laser-excited electrons inside the silica glass. At I = 2.5 x 10^{13} W/cm^2, the primary filament splits into two at a location about 200 μm inside the silica glass. At even higher irradiance (e.g., 10^{14} W/cm^2), filament splitting, as a persistent phenomenon, starts right after the femtosecond laser pulse enters the glass sample.

The nonlinear Schrödinger equation, which is the leading order approximation to the Maxwell's equations, has been successful in describing the propagation of intense laser pulses such as self-focusing in nonlinear Kerr media with nonlinear refractive index n_2. Assuming the laser pulse propagates in the z direction, the basic nonlinear Schrödinger equation has the form [24],

$$2ik\frac{\partial A}{\partial z}+\nabla_{\perp}^{2}A+\frac{2k^{2}n_{2}}{n_{0}}\left|A\right|^{2}A=0\,,$$

where A is the envelope amplitude of the propagating laser electric field, k is the wave vector, $k=\omega n/c$, and $\nabla_{\perp}^{2}$ is the transverse Laplacian operator. The second term represents diffraction, whereas the third term accounts for the contribution due to intensity-dependent refractive index. If the input laser pulse is cylindrically symmetric, according to the nonlinear Schrödinger equation, pulse remains cylindrically symmetric during propagation. As the interpretation of multiple filamentation should include a mechanism that breaks the cylindrical symmetry, the standard explanationof multiple filamentation, developed nearly forty years ago [67], is that breakup of cylindrical symmetry is initiated by small or random inhomogeneity in the input laser pulse. According to this theory, which was based on modulational instability of plane waves that allowed exponential growth of initial perturbations, there is a preferred spatial scale for filaments to form, depending on laser intensity [67].

An alternative deterministic explanation of filament splitting was proposed recently [68] based on nonlinear Schrödinger equation with the inclusion of nonlinear

perturbation that describes self-focusing in the presence of vectorial (polarization) as well as nonparaxial effects. Assuming the input laser pulse is linearly polarized in the *x* direction, the general form of the modified nonlinear Schrödinger equation can be derived as [68],

$$2ik\frac{\partial A}{\partial z}+\nabla_{\perp}^{2}A+\frac{2k^{2}n_{2}}{n_{0}}\left|A\right|^{2}A=f^{2}\Im(A,\frac{\partial A}{\partial x},\frac{\partial^{2}A}{\partial x^{2}})+O(f^{4}),$$

where f (<<1) is the dimensionless parameter defined as the ratio of the laser wavelength to the pulse spot parameter, $f = \lambda / 2\pi r_0$. The asymmetry in the *x* and *y* derivatives of the vectorial perturbation terms in the new equation suggests that the symmetry-breaking mechanism can arise from the vectorial effect for linear polarized laser pulse. This vectorial-induced symmetry breaking leads to multiple filamentation even when the linearly polarized input laser pulse is cylindrically symmetric. **Figure 17** shows a laser pulse profile as it propagates into a Kerr medium at high laser intensity, as calculated using the above modified nonlinear Schrödinger equation [68]. Two filaments emerge that propagate forward in the *z* direction, while moving away from each other along the *x* direction. Multiple filamentation resulting from noise in the input beam should vary between experiments and be independent of the direction of initial polarization, while multiple filamentation resulting from vectorial effects should persist with experiments and depend on polarization.

- ***Temporal splitting***

In addition to spatial splitting, intense femtosecond laser pulse may undergo temporal splitting as it propagates inside a dielectric material [69]. While temporal splitting was predicted theoretically more than ten years ago [70], the experimental verification of temporal splitting was within the last decade [71]. In one such experiment [72], a near-Gaussian 78 fs, 795 nm laser pulse was focused at a 75 μm spot size at the front face of a 3 cm long silica glass sample. The temporal behavior of the pulse was characterized by measuring the intensity cross correlation of the transmitted pulse with the initial input pulse. The spectrum of the transmitted beam was taken concurrently using a fiber-coupled spectrometer with 0.3 nm resolution. **Figure 18** shows the cross

correlation and the corresponding spectrum of the transmitted pulse on axis for pulse intensity above the threshold power for pulse splitting. Associated with temporal splitting, the spectrum of the femtosecond laser pulse can broaden significantly and eventually evolve into supercontinuum or white-light generation at high intensities. Although white-light continuum in transparent dielectrics has been known for decades [73,74], systematic recent experiments revealed that femtosecond laser-induced continuum generation in dielectrics is triggered by self-focusing and depends strongly on the medium's band-gap [75,76].

The nonlinear Schrödinger equation with the inclusion of material dispersion was applied to predict temporal splitting of femtosecond laser pulses inside dielectrics. With the additional group-velocity dispersion term, the nonlinear Schrödinger equation writes [69,72],

$$2ik\frac{\partial A}{\partial z}+\nabla_{\perp}^{2}A-kk''\frac{\partial^{2}A}{\partial\tau^{2}}+\frac{2k^{2}n_{2}}{n_{0}}\left|A\right|^{2}A=0\,,$$

where *k"* is the group-velocity dispersion coefficient, the second derivatives of *k* with respect to laser pulse frequency, and $\tau = t - z/v_g$ is retarded time for pulse moving at group velocity v_g.

Figure 19 shows the calculated pulse intensity surfaces at three propagation distances in fused silica [69]. The femtosecond pulse is initially focused in both space and time as the result of strong self-focusing and the associated pulse sharpening (see section 1.2). As the peak intensity increases, the process of self-phase modulation also increases, which leads to the generation of new frequency components that are red-shifted near the leading edge of the pulse and blue-shifted near the trailing edge. Because of positive group-velocity dispersion in most dielectrics, the wave trains of the laser pulse at different frequencies propagate at different speeds, with the red component faster than the blue. Consequently, the pulse energy is pushed away from $\tau = 0$, initiating pulse splitting.

While the nonlinear Schrödinger equation including normal group-velocity dispersion predicts temporal splitting with symmetry, the asymmetric feature of the

splitting pulses was examined using an equation beyond the slowly varying envelope approximation [72,77]. Self-steepening and space-time focusing were found to shift the beam energy into one of the two split pulses formed by group-velocity dispersion. Similarly, multiphoton ionization and plasma formation were implemented into the modified nonlinear Schrödinger equation. The resulting defocusing and nonlinear absorption of the trailing edge of the pulse tends to push the peak intensity to the leading edge [78]

4. Concluding remarks

While the femtosecond lasers have great potential in processing dielectric materials, the underlying physics is not well understood. We have provided an overview of recent progresses in understanding the fundamental processes of femtosecond laser interactions with dielectrics that are important for materials applications. Two topics discussed in this article include the excitation and relaxation channels of femtosecond laser-induced carriers, and the splitting and self-focusing/defocusing of femtosecond laser pulses inside dielectrics.

Ultrafast imaging and spectral interferometry techniques have been successfully applied to quantify the dynamics of the laser-excited carriers. A significant advancement is the time-resolved detection of de-excitation channels (exciton self-trapping) leading to energy localization from initially delocalized electronic state to a localized lattice. Such a localized carrier relaxation mechanism offers the possibility of defect formation in some perfect dielectrics. In addition to experiments of ultrafast carrier dynamics, also discussed in his article is the challenge in theoretical calculation of femtosecond laser-excited nonequilibrium carriers in materials involving strong electron-phonon coupling.

Self-focusing, defocusing, and spatial splitting (multi-filamentation) of femtosecond laser pulses inside transparent dielectric materials have been examined by ultrafast imaging technique. In the meantime, splitting of femtosecond pulse in the time

domain has also been reported by different research groups. Recent comprehensive theoretical work based on modifications of nonlinear Schrödinger equation has provided much insight into the highly nonlinear processes of spatial and temporal splitting of femtosecond laser pulses propagating inside dielectrics.

The selected topics discussed in this article represent two basic research emphases in the growing field of ultrafast laser interactions with dielectrics. With the continuous advancement of ultrashort pulsed lasers, the maturity of ultrafast imaging, interferometry, and spectroscopic techniques, as well as the rapid growth of computing power and the progress in theoretical understanding of the excited states properties of dielectrics, more subtleties of the nonlinear, nonequilibrium processes during and after femtosecond laser excitation are to be uncovered. It is expected that a thorough understanding of the underlying physics of laser-dielectric interactions will help develop innovative processing technology for traditionally difficult dielectric materials.

References

1. A. H. Zewail, *Femtochemistry: Ultrafast Dynamics of the Chemical Bond* (World Scientific, Singapore, 1994).
2. J. Shah, *Ultrafast Spectroscopy of Semiconductors and Semiconductor Nanostructures* (Springer, Berlin, 1996).
3. C. W. Siders, A. Cavalleri, K. Sokolowski-Tinten, C. Tóth, T. Guo, M. Kammler, M. H. von Hoegen, K. R. Wilson, D. von der Linde, and C. P. J. Barty*, Science* **286,** 1340 (1999).
4. A. Rousse, C. Rischel, S. Foumaux, I. Uschmann, S. Sebban, G. Grillon, Ph. Balcou, E. Förster, J. P. Geindre, P. Audebert, J. C. Gauthier, D. Hulin*, Nature* **410,** 65 (2001).
5. F. Rossi and T. Kuhn, *Rev. Mod. Phys.* **74**, 895 (2002).
6. S. K. Sundaram and E. Mazur, *Nature Materials* **1**, 217 (2002).
7. D. Day, M. Gu, and A. Smallridge, *Opt. Lett*. **24**, 948 (1999).
8. H. Ueki, Y. Kawata, and S. Kawata, *Appl. Opt*. **35**, 2456 (1996).
9. E. N. Glezer, M. Milosavljevic, L. Huang, R. J. Finlay, T.-H. Her, J. P. Callan, and E. Mazur, *Opt. Lett*. **21**, 2023 (1996).
10. M. Watanabe, S. Juodkazis, H.-B. Sun, S. Matsuo, and H. Misawa, *Appl. Phys. Lett*. **77**, 13 (2000).
11. H. Sun, Y. Xu, S. Juodkazis, K. Sun, M. Watanabe, S. Matsuo, H. Misawa, and J. Nishii, *Opt. Lett*. **26**, 325 (2001).
12. L. V. Keldysh, *Sov. Phys. JETP* **20**, 1307 (1965).
13. N. W. Ashcroft and N. D. Mermin, *Solid State Physic*s (Saunders, Philadelphia, 1976).
14. P. Y. Yu and M. Cardona, *Fundamentals of Semiconductor* (Springer, Berlin, 1996).
15. M. V. Fischetti, D. J. DiMaria, S. D. Brorson, T. N. Theis, and J. R. Kirtley, *Phys. Rev.* B **31**, 8124 (1985).
16. D. Arnold and E. Cartier, *Phys. Rev*. B **44**, 10 689 (1991).

17. E. Yablonovitch and N. Bloembergen, *Phys. Rev. Lett.* **29**, 907 (1972).
18. N. Bloembergen, *IEEE J. Quant. Electron*. **10**, 375 (1974).
19. B.C. Stuart, M.D. Feit, S. Herman, A.M. Rubenchik, B.W. Shore, M.D. Perry, *Phys. Rev*. B **53**, 1749 (1996).
20. M. Li, S. Menon, J.P. Nibarger, G.N. Gibson, *Phys. Rev. Lett*. **82**, 2394 (1999).
21. G. Petite, S. Guizard, Ph. Martin, F. Quéré, *Phys. Rev. Lett*. **83**, 5182 (1999).
22. G. L. Yudin, L. N. Gaier, M. Lein, P. L. Knight, P. B. Corkum, M. Yu. Ivanov, submitted to *Laser Physics* (2003).
23. T. Seideman, M. Yu. Ivanov, P. B. Corkum, *Phys. Rev. Lett.* **75**, 2189 (1995).
24. Y. R. Shen, *The principles of Nonlinear Optic*s, (Wiley, New York, 1984).
25. P. L. Kelley, *Phys. Rev. Lett*. **15**, 1005 (1965).
26. J. H. Marburger and W. G. Wagner, *IEEE J. Quantum Electron*. **3**, 415 (1967).
27. K. S. Song and R. T. Williams, *Self-Trapped Excitons* (Springer, Berlin, 1993).
28. R. F. Haglund, Jr. and N. Itoh, in *Laser ablation. Principles and Applications,* ed. J. C. Miller (Springer, Berlin, 1994).
29. M. Ueta, H. Kanzaki, K. Kobayashi, Y. Toyozawa, and E. Hanamura, Eds., *Excitonic Processes in Solids* (Springer, Berlin, 1986).
30. A. N. Vasil'ev, Y. Fang, V. V. Mikhailin, *Phys. Rev*. B **60**, 5340 (1999).
31. Y. Toyozawa, in *Relaxation of Elementary Excitations* (Springer, Berlin, 1980).
32. N. Itoh. *Adv. Phys*. **31**, 491 (1982).
33. A. N. Trukhin, *J. Non-Crystal. Solids* **149**, 32 (1992).
34. T. Sujiyama, H. Fujiwara, T. Suzuki, K. Tanimura, *Phys. Rev*. B **54**, 15109 (1996).
35. E. D. Thoma, H. M. Yochum, and R. T. Williams, *Phys. Rev*. B **56**, 8001 (1997).
36. S. Guizard, Ph. Martin, G. Petite, P. D 'Oliveira, P. Maynadier, *J. Phys. Condens. Matter* **8**, 1281 (1996).

37. I. Tanimura, T. Tanaka, and N. Itoh**,** *Phys. Rev. Lett.* **51**, 423 (1983).
38. M. Lenzner, *Int. J. Mod. Phys*. B **13**, 1559 (1999).
39. A.-C. Tien, S. Backus, H. Kapteyn, M. Murnane, G. Mourou, *Phys. Rev. Lett*. **82**, 3883 (1999).
40. A. Kaiser, B. Rethfeld, M. Vicanek, and G. Simon, *Phys. Rev.* B **61**, 11437, (2000).
41. R. Stoian, D. Ashkenasi, A. Rosenfeld, and E. E. B. Campbell, *Phys. Rev.* B **62**, 13167 (2000).
42. R. Stoian, A. Rosenfeld, D. Ashkenasi, I. V. Hertel, N. M. Bulgakova, and E. E. B. Campbell, *Phys. Rev. Lett.* **88**, 097603 (2002).
43. Note here that an important energy relaxation mechanism, known as "plasmon losses", has been so far disregarded in the models of laser interaction with dielectrics despite the fact that it is well documented in both theoretical and experimental works on energy losses in dielectrics.
44. X. Mao, S. S. Mao, and R. E. Russo, *Appl. Phys. Lett*. **82**, 697 (2003).
45. C. Iaconis, I.A. Walmsley, *Opt. Lett.* **23,** 792 (1998).
46. F. Quéré, J. Itatani, G. L. Yudin and P. B. Corkum, *Phys. Rev. Lett.,* **90**, 73902 (2002).
47. J.P. Geindre, P. Audebert, S. Rebibo, J.-C. Gauthier, *Opt. Lett.* **26,** 1612 (2001).
48. S. S. Mao, X. Mao, R. Greif, and R. E. Russo, *Appl. Phys. Lett.* **77**, 2464 (2000).
49. Ph. Martin, S. Guizard, P. Daguzan, G. Petite, P. D'Oliviera, P. Meynadier, M. Perdrix, *Phys. Rev. B* **55**, 5799 (1997).
50. F. Quéré, S. Guizard, Ph. Martin, *Europhys. Lett.* **56**, 138 (2001).
51. K. Tanimura and H. Fujiwara, *Proceedings of 13th ICDIM* (Wiston-Salem, July 1996), in "Material Science Forum", **239-241**, 549, H. G. Mattews and R. T. Williams editors (Trans Tech., Zurich, 1997).
52. R. T. Williams, B. B. Craig and W. L. Faust, *Phys. Rev. Lett.* **52**, 1709 (1984).
53. T. Shibata, S. Iwai, T. Tokisaki, K. Tanimura, A. Nakamura and N. Itoh; *Phys. Rev.* B **49**, 13255 (1994).

54. G. D. Mahan, *Many particles physics* (Plenum press, New York, 1990).
55. P. Daguzan, Ph. Martin, S. Guizard, and G. Petite, *Phys. Rev.* B **52**, 17099 (1995).
56. H. J. Kreuzer, *Non-equilibrium Thermodynamics and its Statistical Foundations* (Clarendon, Oxford, 1981).
57. H. Frölich, *Adv. Phys.* **3**, 325 (1954).
58. J. Schilp, T. Kuhn and G. Mahler, *Phys. Rev.* B **50**, 5435 (1994).
59. H. Haug and S.W. Koch, *Quantum theory of the optical and electronic properties of semi conductors* (World Scientific, New York, 1993).
60. G. Onida, L. Reining, A. Rubio, *Rev. Mod. Phys.* **74**, 601 (2002).
61. E. Runge and J. F. Gross, *Phys. Rev. Lett.* **52**, 997 (1984).
62. A. Braun, G. Korn, X. Liu, D. Du, J. Squier, and G. Mourou, *Opt. Lett*. **20**, 73 (1995).
63. A. Brodeur, O. G. Kosareva, C. Y. Chien, F. A. Ilkov, V. P. Kandidov, and S. L. Chin, *Opt. Lett*. **22,** 304 (1997).
64. B. La Fontaine, F. Vidal, Z. Jiang, C. Y. Chien, D. Comtois, A. Desparois, T. W. Johnston, J.-C. Kieffer, and H. Pepin, H. P. Mercure, Phys. Plasmas **6**, 1615 (1999).
65. S. Tzortzakis, L. Sudrie, M. Franco, B. Prade, A. Mysyrowicz, A. Couairon and L. Bergé, *Phys. Rev. Lett*. **87**, 3902 (2001).
66. S. Henz and J. Herrmann, *Phys. Rev*. A **59**, 2528 (1999).
67. V. I. Bespalov and V. I. Talanov, *JETP Lett*. **3,** 307 (1966).
68. G. Fibich and B. Ilan, *Physica* D **157**, 113 (2001).
69. S. A. Diddams, H. K. Eaton, A. A. Zozulya, and T. S. Clement, *IEEE J. Select. Top. Quan. Electro*. **4**, 306 (1998).
70. J. E. Rothenberg, *Opt. Lett.* **17**, 583 (1992).
71. J. Ranka, R. W. Schirmer, and A. Gaeta, *Phys. Rev. Lett.* **77**, 3783 (1996).
72. J. K. Ranka and A. L. Gaeta, *Opt. Lett*. **23**, 534 (1998).
73. R. R. Alfano and S. L. Shapiro, *Phys. Rev. Lett.* **24**, 584 (1970).
74. G. Y. Yang and Y. R. Shen, *Opt. Lett.* **9**, 510 (1984).
75. A. Brodeur and S. L. Chin, *Phys. Rev. Lett.* **80**, 4406 (1998).

76. A. Brodeur and S. L. Chin, *J. Opt. Soc. Am.* **B16**, 637 (1999).
77. A. A Zozulya S. A. Diddams, A. G. Van Engen, and T. S. Clement, *Phys. Rev. Lett*. **82**, 1430 (1999).
78. A. L. Gaeta, *Phys. Rev. Lett*. **84**, 3582 (2000).

Figure Captions

Figure 1. Schematic illustration of (a) multiphoton ionization, (b) free carrier absorption, and (c) impact ionization [6].

Figure 2. Schematic illustration of 100 fs laser-induced electron density evolution under three different excitation-relaxation conditions: multiphoton ionization only, multiphoton plus avalanche ionization, multiphoton plus avalanche ionization with carrier trapping. Multiphoton ionization provides seed electrons for avalanche ionization, whereas trapping offers a channel for electron density reduction. The Gaussian laser pulse is also illustrated.

Figure 3. Schematic illustration of (a) self-focusing and (b) self-phase modulation resulting from a nonlinear refractive index.

Figure 4. Schematic illustration of exciton level and two basic routes for exciton generation: (a) inelastic scattering of the multiphoton-excited electrons and (b) direct resonant absorption of multiple photons.

Figure 5. Schematic illustration of defect formation from self-trapped excitons. (a) an on-center self-trapped exciton, (b) an off-center self-trapped exciton, and (c) an F-H pair in alkali halides. Small and large circles represent alkali and halogen ions, respectively.

Figure 6. Schematic illustration of exciton and intrinsic defect energy levels in SiO_2.

Figure 7. Femtosecond (800 nm) laser-induced damage threshold in fused silica. Data from reference [39].

Figure 8. (a) Time-resolved images of femtosecond laser-induced electronic excitation inside a silica glass; (b) evolution of electron number density profile inside a femtosecond laser-irradiated silica glass.

Figure 9. Experimental set-up for spectral interferometry. The probe beam waist is larger than the pump beam waist (typically 10 μm), and the interaction area is imaged on the entrance slit of the spectrometer with a large magnification, so that the spatial profile of phase shift along the slit direction (r) is obtained.

Figure 10. Temporal evolution of phase shift in MgO and SiO_2 (800 nm pump with an intensity well below the breakdown threshold, 400 nm probe). The arrows indicate the delays where the intensity dependences of phase shift in these two materials were measured.

Figure 11. Intensity dependence of the phase shift ($\Delta\Phi_\infty$) after the pump (see arrows in previous figure), for an 800 nm pump, in MgO and SiO_2. The full lines indicate the power laws obtained at low intensity. The vertical dotted line shows the breakdown threshold measured in SiO_2 for a 60 fs, 800 nm pulse [19].

Figure 12. Rise time of the 5.2 eV absorption band of the SiO_2 STE.

Figure 13. Typical time-resolved absorption spectra measured in KCl at two temperatures. At 6K, only the STE absorption is observed while at 80 K, one sees evidence of the transformation of some STE in a permanent F-center [51].

Figure 14. Comparison of semi-classical and quantum approaches in calculating average electron energy as a function of time.

Figure 15. Maximum electron density as a function of time as a femtosecond laser pulse (100 fs, 800 nm) propagates inside a silica glass.

Figure 16. Intensity dependence of femtosecond laser-induced electronic excitation inside a silica glass.

Figure 17. Calculated pulse splitting as a femtosecond laser propagates inside a dielectric material. The letters in the figure indicate the normalized propagation distance (A through F: z = 0, 0.11, 0.14, 0.17, 0.22, 0.4) [68].

Figure 18. Experimentally measured (a) cross correlation and (b) power spectra of the pulses transmitted through a 3-cm fused-silica glass sample with a peak power 5.1 MW. The dashed curves in (a) and (b) are the autocorrelation and the spectrum of the input pulse, respectively [72].

Figure 19. Theoretical pulse intensity surface plots of a femtosecond pulse at three different propagation lengths: (a) input; (b) z = 2.0 cm; and (c) z = 3.0 cm. The pulse intensities were normalized by the peak value [69].

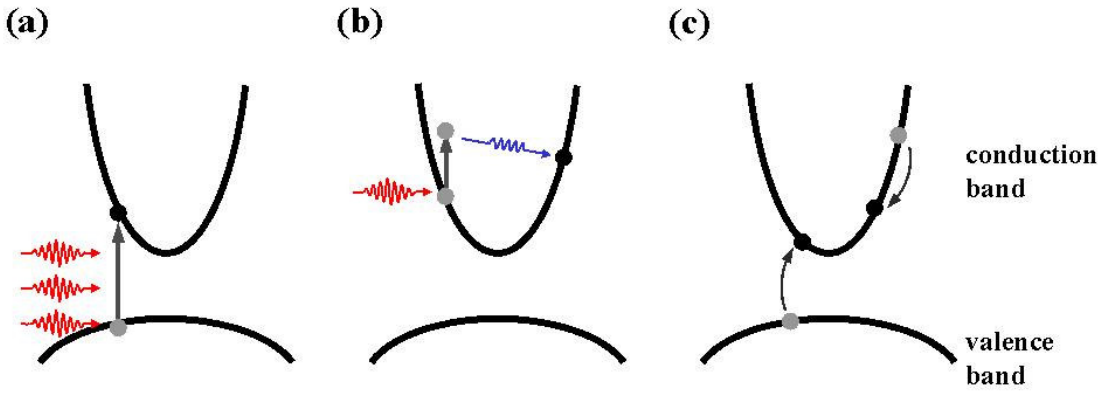

Fig.1

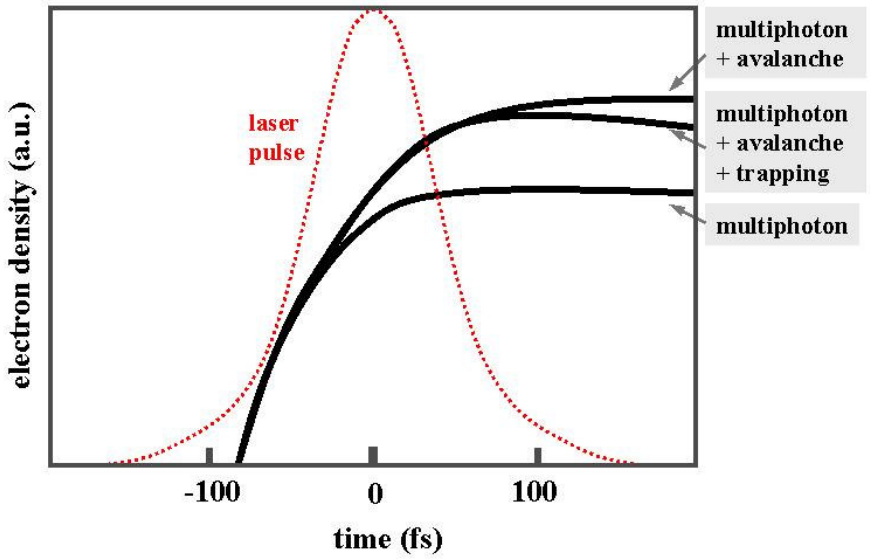
multiphoton
+ avalanche
multiphoton
+ avalanche
+ trapping
multiphoton
laser
pulse
electron density (a.u.)
-100
0
100
time (fs)

Fig.2

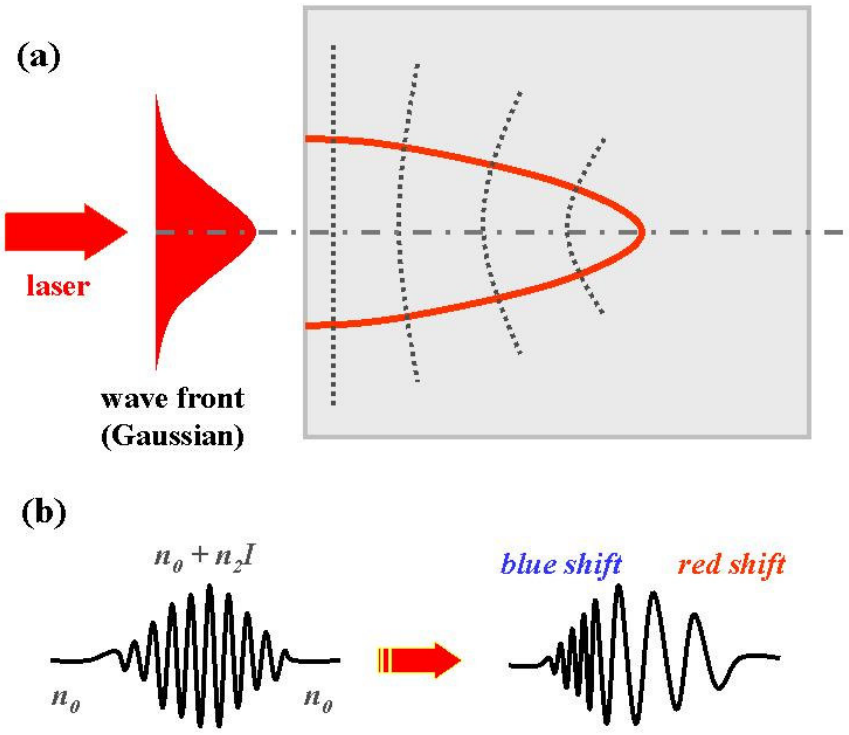
(a)
laser
wave front
(Gaussian)
(b)
$n_0 + n_2 I$
n_0
n_0
blue shift
red shift

Fig.3

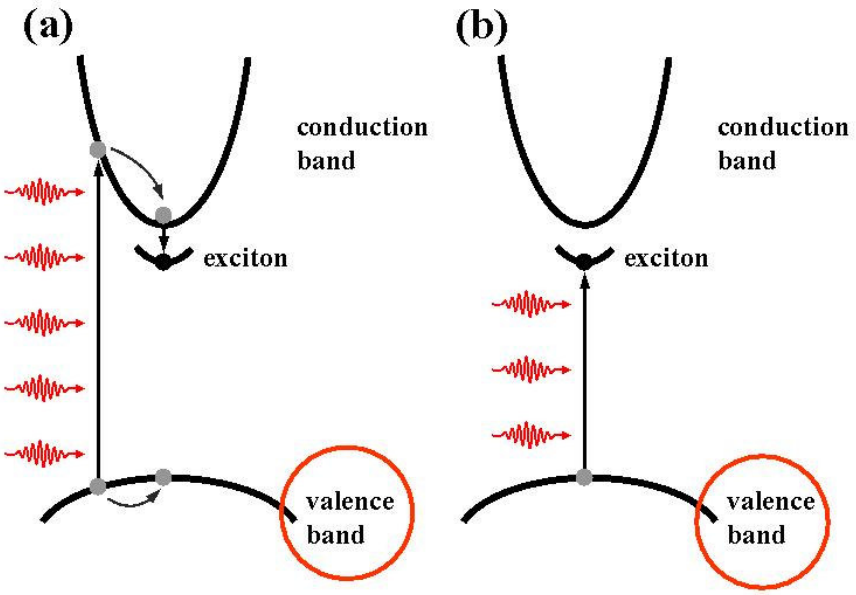
(a)
conduction band
exciton
valence band
(b)
conduction band
exciton
valence band

Fig.4

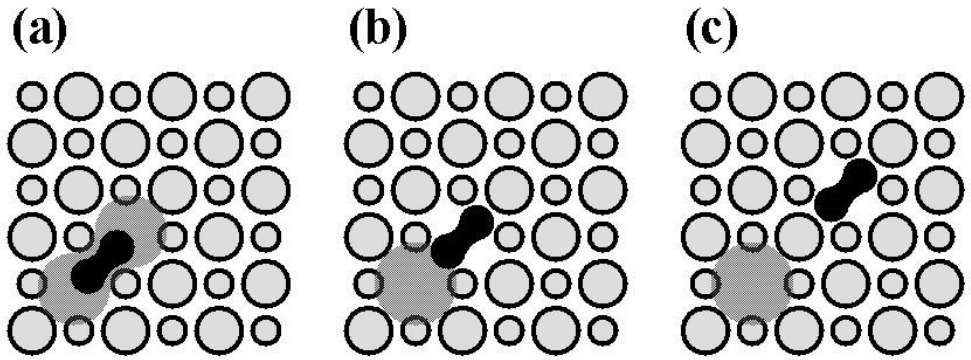

Fig.5

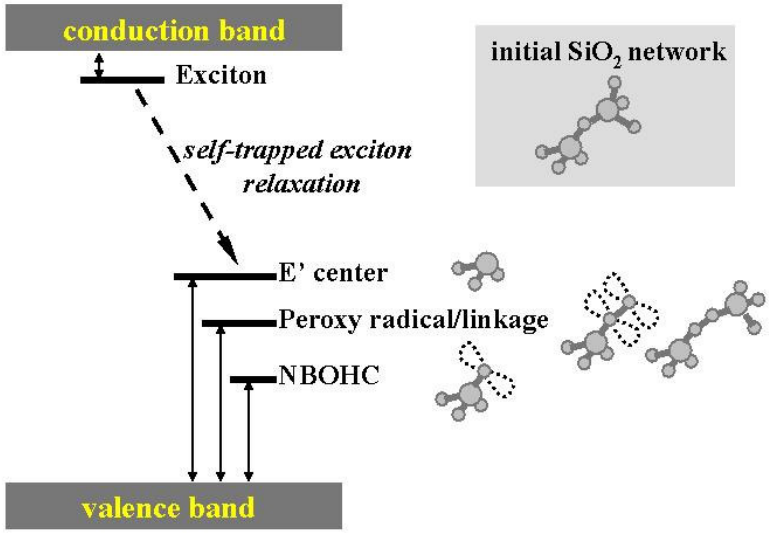
conduction band
Exciton
self-trapped exciton
relaxation
initial SiO_2 network
E' center
Peroxy radical/linkage
NBOHC
valence band

Fig.6

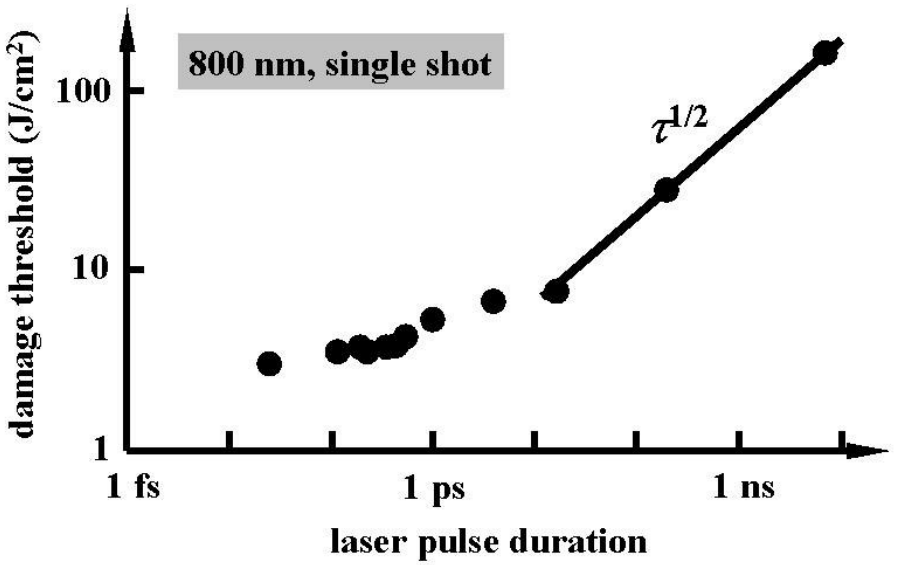
800 nm, single shot
damage threshold (J/cm²)
100
10
1
τ^1/2
1 fs
1 ps
1 ns
laser pulse duration

Fig.7

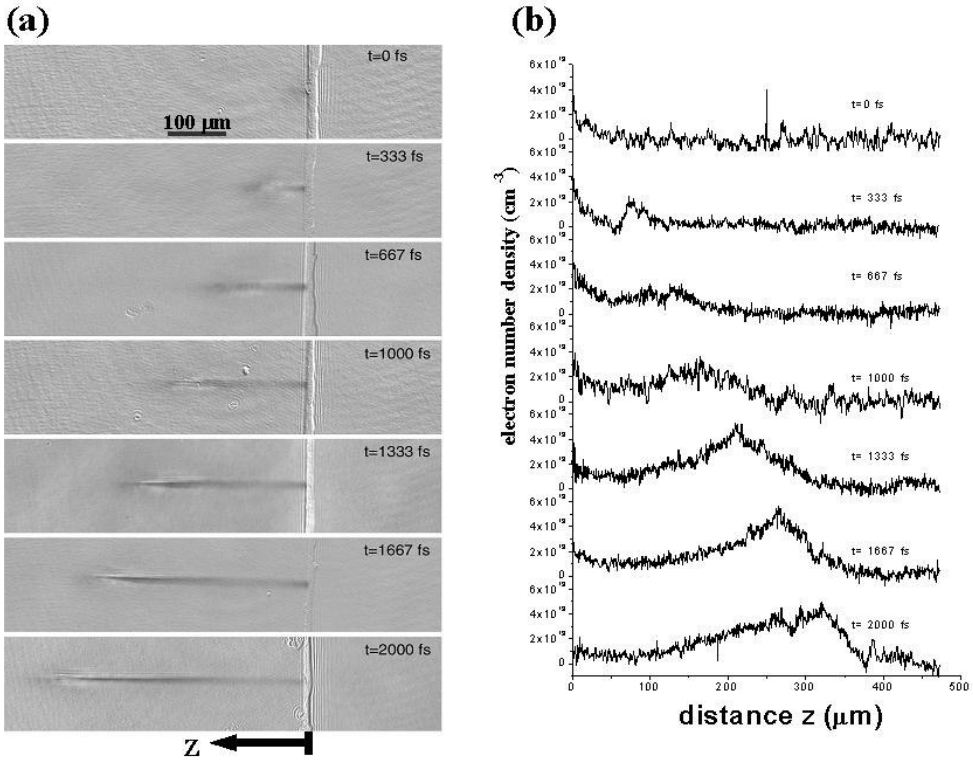
(a)
t=0 fs
100 μm
t=333 fs
t=667 fs
t=1000 fs
t=1333 fs
t=1667 fs
t=2000 fs
Z
(b)
electron number density (cm-3)
t= 0 fs
t= 333 fs
t= 667 fs
t= 1000 fs
t= 1333 fs
t= 1667 fs
t= 2000 fs
distance z (μm)

Fig.8

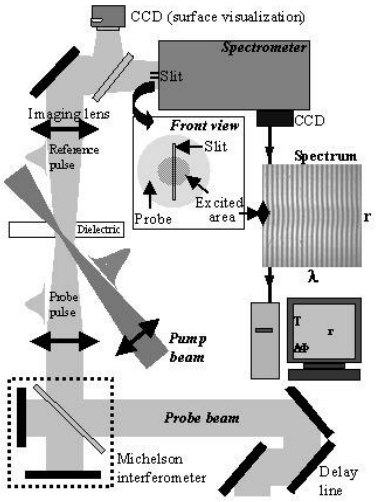
CCD (surface visualization)
Spectrometer
Slit
Imaging lens
CCD
Front view
Slit
Reference pulse
Spectrum
Excited area
Probe
r
Dielectric
λ
Probe pulse
T
r
Pump beam
Probe beam
Michelson interferometer
Delay line

Fig.9

Warning : Figure modified !

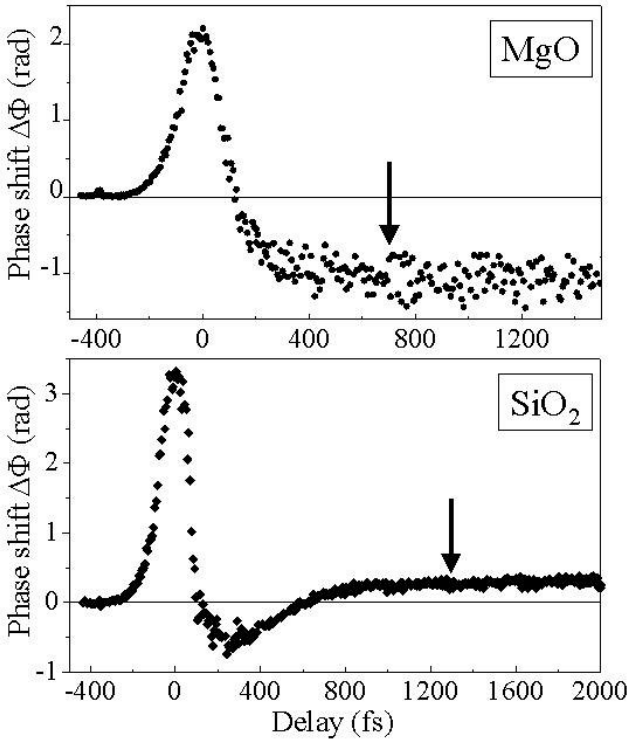

Fig.10

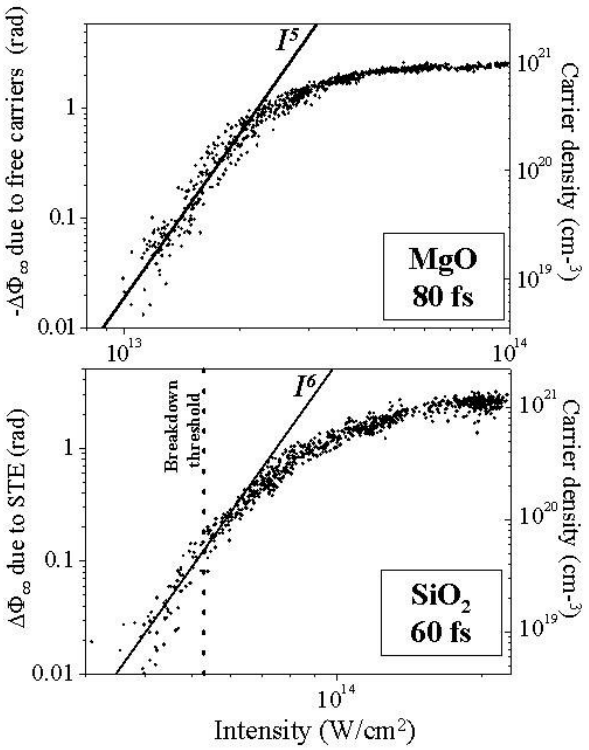
I^5
MgO
80 fs
$-\Delta\Phi_\infty$ due to free carriers (rad)
Carrier density (cm^{-3})
I^6
Breakdown threshold
SiO_2
60 fs
$\Delta\Phi_\infty$ due to STE (rad)
Intensity (W/cm^2)

Fig.11

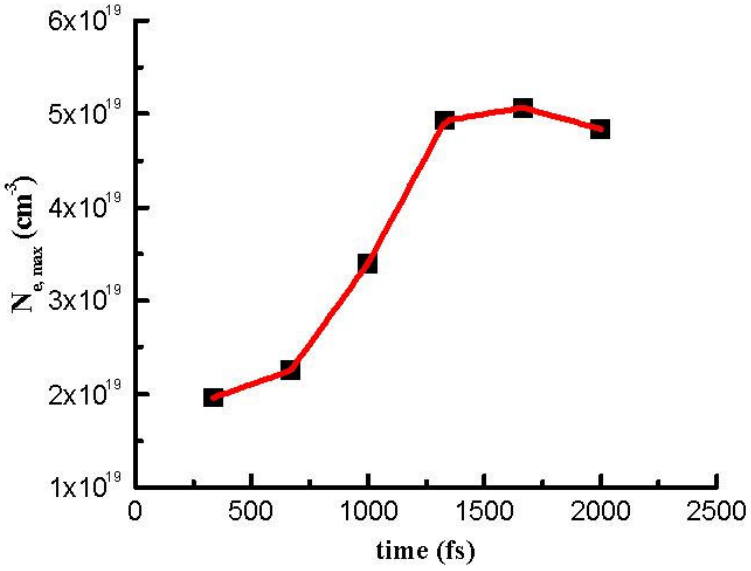
6x10^19
5x10^19
4x10^19
3x10^19
2x10^19
1x10^19
N_e, max (cm^-3)
0
500
1000
1500
2000
2500
time (fs)

Fig.12

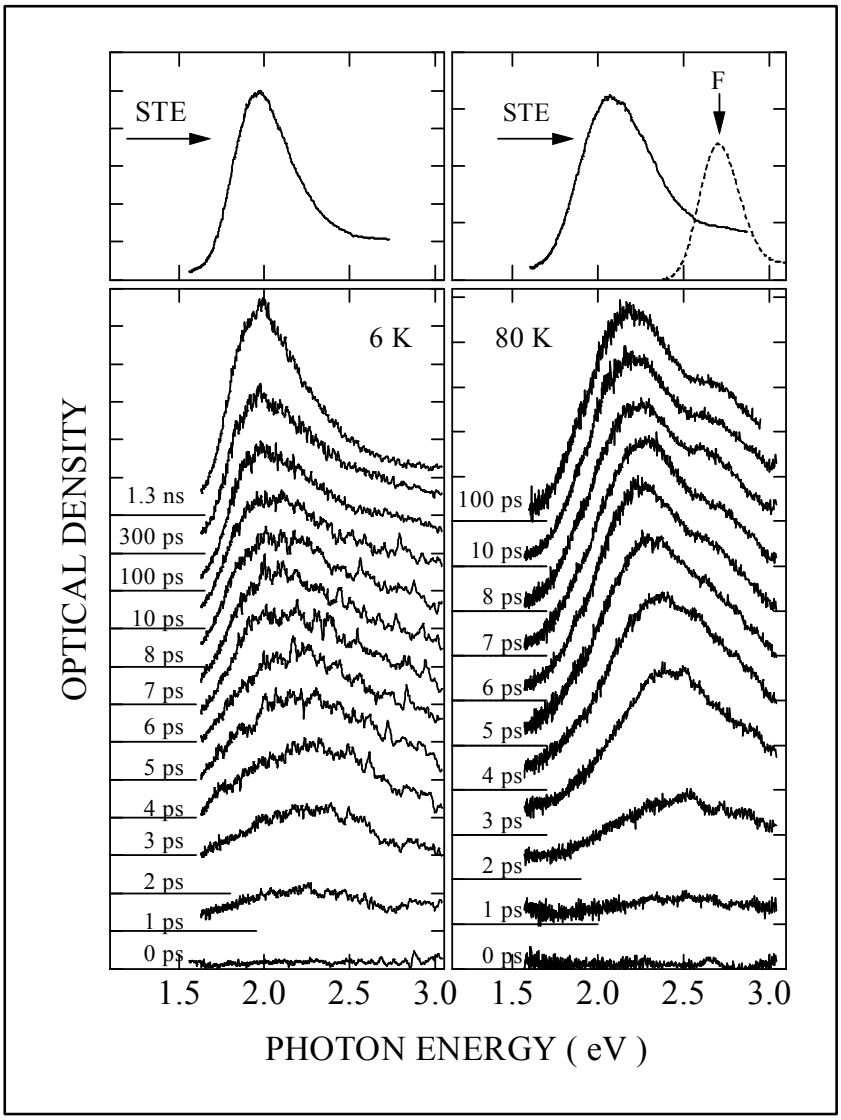
STE
STE
F
6 K
80 K
1.3 ns
300 ps
100 ps
10 ps
8 ps
7 ps
6 ps
5 ps
4 ps
3 ps
2 ps
1 ps
0 ps
100 ps
10 ps
8 ps
7 ps
6 ps
5 ps
4 ps
3 ps
2 ps
1 ps
0 ps
OPTICAL DENSITY
1.5
2.0
2.5
3.0
1.5
2.0
2.5
3.0
PHOTON ENERGY (eV)

Fig. 13

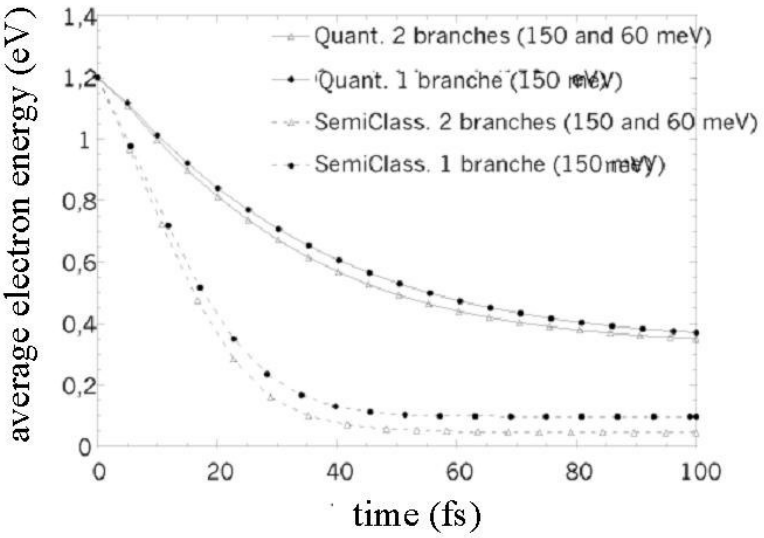
average electron energy (eV)
time (fs)
Quant. 2 branches (150 and 60 meV)
Quant. 1 branche (150 meV)
SemiClass. 2 branches (150 and 60 meV)
SemiClass. 1 branche (150 meV)
0
0,2
0,4
0,6
0,8
1
1,2
1,4
0
20
40
60
80
100

Fig.14

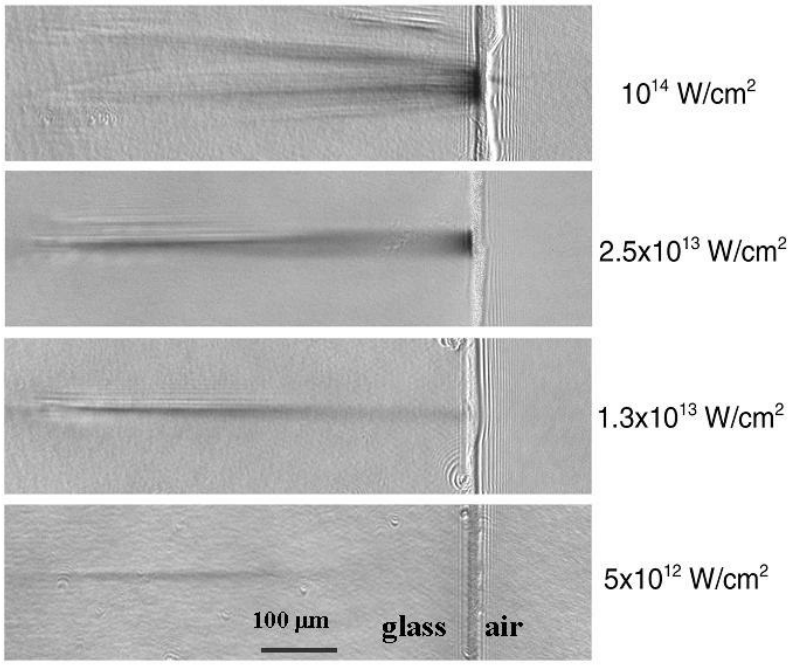
10^{14} W/cm^2
2.5x10^{13} W/cm^2
1.3x10^{13} W/cm^2
5x10^{12} W/cm^2
100 μm
glass
air

Fig.15

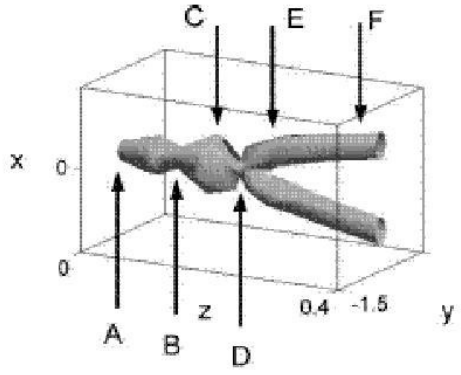

Fig.17

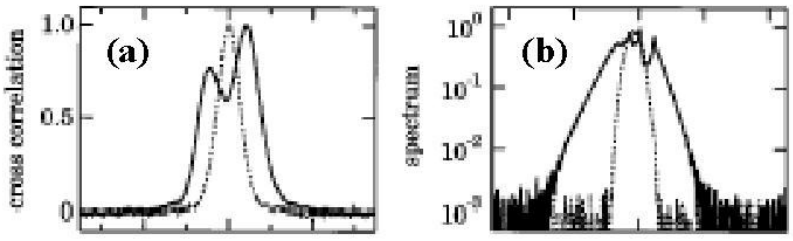

Fig.18

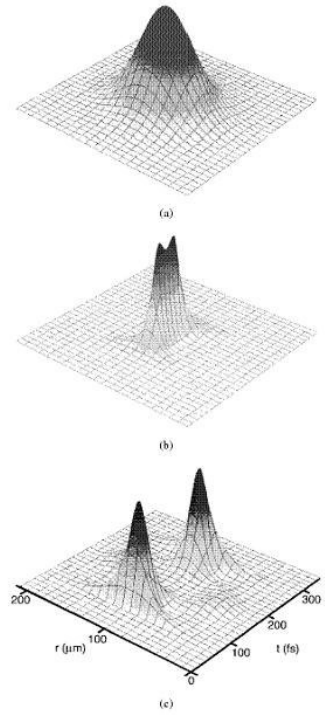

Fig.19